ADVANCED HEALTHCARE MATERIALS
www.advhealthmat.de

Uniaxial and Coaxial Vertical Embedded Extrusion Bioprinting

Liming Lian, Cuiping Zhou, Guosheng Tang, Maobin Xie, Zixuan Wang, Zeyu Luo, Julia Japo, Di Wang, Jianhua Zhou, Mian Wang, Wanlu Li, Sushila Maharjan, Marina Ruelas, Jie Guo, Xunwei Wu, and Yu Shrike Zhang**

The 3D bioprinting technologies have attracted increasing attention due to their flexibility in producing architecturally relevant tissue constructs. Here, a vertical embedded extrusion bioprinting strategy using uniaxial or coaxial nozzles is presented, which allows formation of vertical structures of homogeneous or heterogeneous properties. By adjusting the bioprinting parameters, the characteristics of the bioprinted vertical patterns can be precisely controlled. Using this strategy, two proof-of-concept applications in tissue biofabrication are demonstrated. Specifically, intestinal villi and hair follicles, two liner-shaped tissues in the human body, are successfully generated with the vertical embedded bioprinting method, reconstructing some of their key structures as well as restoring partial functions in vitro. Caco-2 cells in the bioprinted intestinal villus constructs proliferated and aggregated properly, also showing functional biomarker expressions such as ZO-1 and villin. Moreover, preliminary hair follicle structures featuring keratinized human keratinocytes and spheroid-shaped human dermal papilla cells are formed after vertical bioprinting and culturing. In summary, this vertical embedded extrusion bioprinting technique harnessing a uniaxial or coaxial format will likely bring further improvements in the reconstruction of certain human tissues and organs, especially those with a linear structure, potentially leading to wide utilities in tissue engineering, tissue model engineering, and drug discovery.

1. Introduction

The 3D bioprinting technologies allow for fabrication of sophisticated tissue architectures, facilitating improvements in medical treatments and healthcare, especially in areas such as organ transplantation, regenerative engineering, and drug screening.[1–5] So far, there are various bioprinting technologies developed, including but not limited to inkjet bioprinting,[6] extrusion bioprinting,[7–9] and vat-polymerization bioprinting.[10,11] Current bioprinting techniques have demonstrated their widespread use in engineering a variety of tissues. However, they are mostly based on a layer-by-layer method[12], which makes it difficult to produce high-aspect ratio vertical and hollow structures that are sometimes required for engineering certain tissue types or subunits. The intestinal villi[13] and the hair follicles[14] are two examples of linear tissue units that feature vertically arranged array structures at high aspect ratios and heterogeneous properties.

L. Lian, C. Zhou, G. Tang, M. Xie, Z. Wang, Z. Luo, J. Japo, D. Wang, J. Zhou, M. Wang, W. Li, S. Maharjan, M. Ruelas, J. Guo, Y. S. Zhang
Division of Engineering in Medicine
Department of Medicine
Brigham and Women's Hospital
Harvard Medical School
Cambridge, MA 02139, USA
E-mail: yszhang@research.bwh.harvard.edu

C. Zhou
Department of Emergency
Nanfang Hospital
Southern Medical University
Guangzhou 510515, P. R. China

G. Tang
NMPA & Guangdong Key Laboratory of Molecular Target & Clinical Pharmacology
State Key Laboratory of Respiratory Disease
School of Pharmaceutical Sciences
The Fifth Affiliated Hospital
Guangzhou Medical University
Guangzhou, Guangdong 511436, P. R. China

X. Wu
Cutaneous Biology Research Center
Massachusetts General Hospital
Harvard Medical School
Boston, MA 02129, USA
E-mail: xunwei.wu@cbrc2.mgh.harvard.edu

The ORCID identification number(s) for the author(s) of this article can be found under https://doi.org/10.1002/adhm.202102411

DOI: 10.1002/adhm.202102411

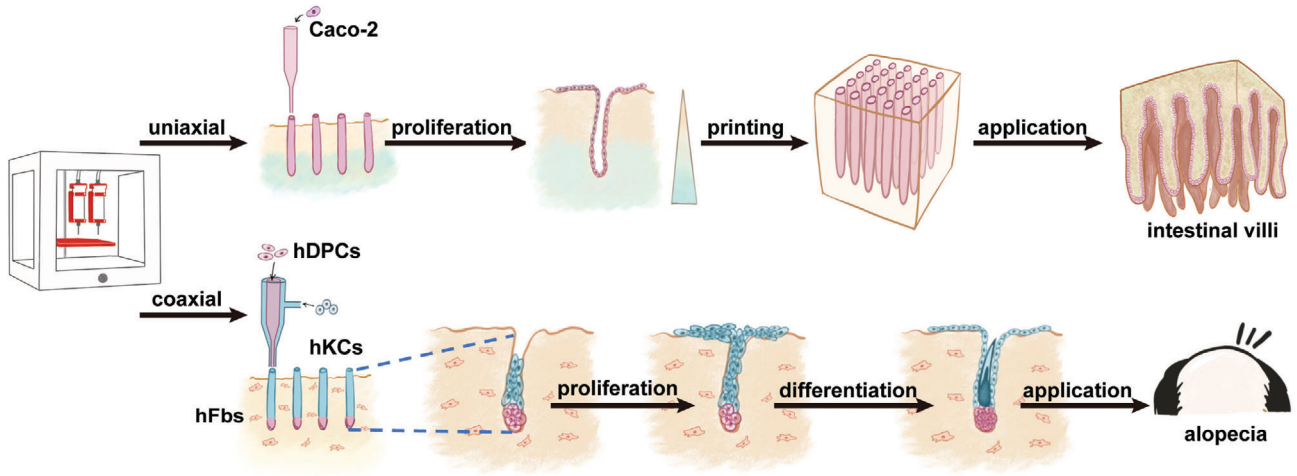

Scheme 1. Scheme showing the uniaxial vertical embedded bioprinting strategy to reconstruct tissue units such as the intestinal villi in a dual-layer support base, or the coaxial vertical embedded bioprinting strategy to reconstruct tissue units such as the human hair follicles in a multisegment filament manner.

It is well-known that these vertical and oftentimes hollow structures such as the intestinal villi and hair follicles, play important roles in the human body.[15,16] For instance, every year millions of patients in the US suffer digestive disorders due to abnormalities in intestinal epithelium,[17] and similar numbers of people in the US experience severe skin exfoliation or disfigurement due to heat and pressure injuries, chronic diabetic ulcers, or hereditary vesicular skin diseases.[18] However, present commonly used techniques for intestinal villus and hair follicle engineering are primarily based on photolithography[19] or soft lithography,[14,20] which can regenerate the topographies of these two structures, but usually require more complicated processes and may involve limited efficiency.[14,21] Moreover, both intestinal villi and hair follicles are surrounded by complex microenvironments such as microenvironment gradients (e.g., in intestinal villi)[22] and intensive cell–cell interactions (e.g., dermal papilla–epidermal cell interactions in hair follicles).[23] Consequently, a versatile 3D bioprinting strategy that can perform single- or multimaterial tissue fabrication,[24,25] in particular in the vertical manner synergized with cytocompatible microenvironments could be beneficial to addressing the above-mentioned challenges.

Of interest, embedded bioprinting is a recently exploited extrusion bioprinting modality aiming to solve technical limitations associated with conventional extrusion bioprinting to act against gravity.[26–29] Bioinks utilized in most bioprinting applications are soft and mechanically weak to support high printing fidelity.[30,31] Therefore, it is oftentimes difficult to accurately form complex 3D tissue structures using conventional bioprinting strategies including that based on extrusion. The cell-laden support base used in embedded bioprinting not only provides an in vitro microenvironment, but also facilitates assembly of bioinks at decent fidelity and precision.[9] Embedded bioprinting, by allowing extrusion of soft bioink(s) into a support matrix, could enable truly freeform 3D extrusion bioprinting of sophisticated architectures without having to worry about their collapse during the fabrication process without the support bath.

Here, we report an enabling yet simple variation of embedded extrusion bioprinting, via the utilization of a uniaxial or coaxial nozzle system to produce arrays of high-aspect ratio vertical filaments, to fabricate tissues of linear structures in nature (**Scheme 1**). Specifically, a single-axial nozzle could be used to bioprint vertical filament arrays in a heterogeneous support matrix, as an example, a dual-layer matrix of Caco-2 cell-laden villus-like structures. In the human intestinal system, to support the survival of anaerobes in the colon, the areas of villi in direct contact with the colonic lumen are typically hypoxic,[32] while the microenvironment at the villus bases is normoxic due to high turnover of substances,[33] mostly caused by the varying densities of vascular networks in these different regions.[34] Because the microenvironment is partially influenced by the concentration of the matrix, or gelatin methacryloyl (GelMA) used in our study,[35] the two layers in the support base possessing differential properties might mimic this changing microenvironment along the length of the bioprinted hollow villi, formed by liquefying the extruded vertical filaments of gelatin.[22] By optimizing the bioprinting parameters, including nozzle moving speed, concentration of cells mixed in the bioink, and concentrations of materials in the support base, we could obtain the intestinal villi equipped with similar shape and dimension to their native counterparts in human (≈200 μm in diameter and ≈2 mm in length).[36] After culturing within the heterogeneous microenvironment, positive and differential Caco-2 cellular activities such as cell aggregation, viability, proliferation, morphology, and biomarker expressions, were apparent.

For hair follicle bioprinting, we followed the procedure briefed in the lower portion of Scheme 1. Using the customized coaxial nozzle allowed us to sequentially deposit two types of bioinks, composed of human dermal papilla cell (hDPC)-laden GelMA and human keratinocyte (hKC)-laden gelatin, respectively, during the single extrusion process. Different with previous studies where only single bioinks could be bioprinted one at a time in the embedded bioprinting setup, our coaxial vertical embedded bioprinting strategy would allow convenient, fast dual-material

bioprinting in the vertical direction. As such, certain types of cell–cell interactions in vivo are reproducible, including efficiently promoting the aggregation and differentiation of hDPCs and hKCs in different vertical segments both embedded in the surrounding human dermal fibroblast (hFb)-laden support base (GelMA). Compared to the fact that hair-inductivity of hDPCs usually disappears rapidly in 2D cultures[37] and the unstructured 3D spheroid cultures,[14] our 3D-bioprinted segments featuring photocrosslinkable GelMA was anticipated to shorten the aggregation process of hDPCs inside. In addition, the bioprinted gelatin segment mixed with hKCs acted as a sacrificial bioink, which would melt and likely diffuse out of the microchannels after culturing at 37 °C, during which the hKCs could stay, attach to the microchannel surface, proliferate, and differentiate rapidly, as well as interact with the hDPCs at the bottom and hFbs at the surrounding. Immuno(histo)chemistry results indicated that the bioprinted tissue developed a preliminary, hair follicle-like structure.

2. Results and Discussions

2.1. Printability of the (Bio)inks

As shown in **Figure 1**A, the gelatin (bio)inks at different concentrations presented obviously different printability in the support bases of different GelMA concentrations. In Figure 1A, the 1% gelatin (bio)ink presented the worst printability, where continuous lines could not be extruded in all GelMA support bases. In contrast, the 3% (bio)ink resulted in continuous and uniform structures in all GelMA support bases. Although the 5% (bio)ink also formed filaments, their surfaces were less smooth, and their diameters were less uniform compared with the printing performances of the 3% (bio)ink. The printability map (Figure 1B) clearly illustrated that the 3% gelatin (bio)ink might be the best choice for this vertical embedded printing procedure. The quantified diameters of the vertically printed gelatin filaments shown in Figure 1C revealed that, the diameter increased with the decline of the concentration of GelMA in the support base; the diameter also increased when the gelatin (bio)ink concentration was increased. These observations were likely associated with the alterations in the mechanical properties of the gels when their concentrations were changed, as we extensively demonstrated before.[30,31] They also provided us a general idea regarding how to optimize the printing parameters in the multimaterial configurations for modeling the target tissues later on.

For GelMA (bio)inks (Figure 1D), except for 10%, both 3% and 7% GelMA (bio)ink could print good structures in the 3% GelMA support base. Compared with the performances of 3% and 10% GelMA (bio)inks printed in the 7% GelMA support base, the 7% GelMA (bio)ink showed extrusion of better vertical lines. Moreover, none of the concentrations (3%, 7%, and 10%) embed-printed in the 10% GelMA support base produced good shapes. The observations were summarized in the printability map shown in Figure 1E. The trends in the extruded filament diameters were similar to those for the gelatin (bio)inks, showing a (bio)ink and support bath concentration-dependent behavior (Figure 1F).

Our data suggested that the fidelity and accuracy of the printing results relied on the properties of both the (bio)ink and the support base, consistent with those reported elsewhere.[38–49] The (bio)ink or support base with inadequate performances would lead to instable printing processes, such as discontinuous (bio)ink flows and rough surfaces of extruded filaments. In addition, unwanted interdiffusion of the materials and nonuniform lines could become possible.

2.2. Intestinal Villus Bioprinting

We adopted 3% gelatin as the sacrificial bioink mixed with Caco-2 cells for vertical embedded bioprinting of intestinal villi. We chose gelatin as the bioink due to the ability to liquefy it post-bioprinting to leave the hollow channels allowing attachment and growth of the cells forming the villus-like structures.[40] According to the printability evaluations, we expected that different moving speeds of the nozzle could be utilized in different GelMA support bases aiming to control the diameters of the filaments extruded to be roughly the same. As shown in **Figure 2**A, different combinations of GelMA support bases and different moving speeds of the nozzle were set to understand and optimize the printing performances. Take the support base combining 7% GelMA in the lower layer and 10% GelMA in the upper layer for example, the speed we used in the lower layer was 3 mm s^{-1} while that for the upper layer was 2 mm s^{-1}, which led to continuous vertical filament with similar diameters in the two layers when compared with printing using the same speed (Figure 2B,C). Furthermore, by comparing the differences of diameters in the two layers of all groups, it was found that printing with the abovementioned parameters produced a vertical structure with a diameter close to the real intestinal villi (100–200 μm in diameter).[36]

Caco-2 cells are extensively used as a model of the intestinal barrier for applications in drug screening and tissue engineering.[41,42] Thus, for the purpose of mimicking a partially functional intestinal villus structure, we first examined the Caco-2 cell growth in our 3D-bioprinted constructs. After printing with the bioink (3% gelatin mixed with 1×10^7 cells mL^{-1} of Caco-2 cells) (Figure S1, Supporting Information), we determined the cell viability for up to 14 days of culture. As suggested in Figure 2D and Figure S2 of the Supporting Information, the live (green) and dead (red) images illustrated that few dead cells were present in the samples, and the cells proliferated well. Specifically, the cell viability was quantified at over 95% for all time points evaluated (Figure 2E); the cell proliferation ratio normalized to the value of day 1 was 244.95 ± 23.79% at day 14, which obviously increased compared with day 3 (139.14 ± 13.51) and day 5 (155.04 ± 15.06) (Figure 2F).

Moreover, aiming to determine the influence of different layers of the support bath on the growth of Caco-2 cells, the live and dead images were separated into two parts (lower layer (7% GelMA) and upper layer (10% GelMA)) as illustrated by the dashed red lines in Figure 2D. After we calculated the relatively fluorescence intensity (fluorescence intensity of the upper layer divided by that of the lower layer) of each time point, we found that the cells in the lower layer grew and proliferated much better than those in the upper layer (Figure 2G). The comparison of F-actin staining of cells in the two different layers on days 1, 7, and 14 also led to the same conclusion (Figure 2H and Figure S3A, Supporting Information). The microenvironment in a hydrogel relies on

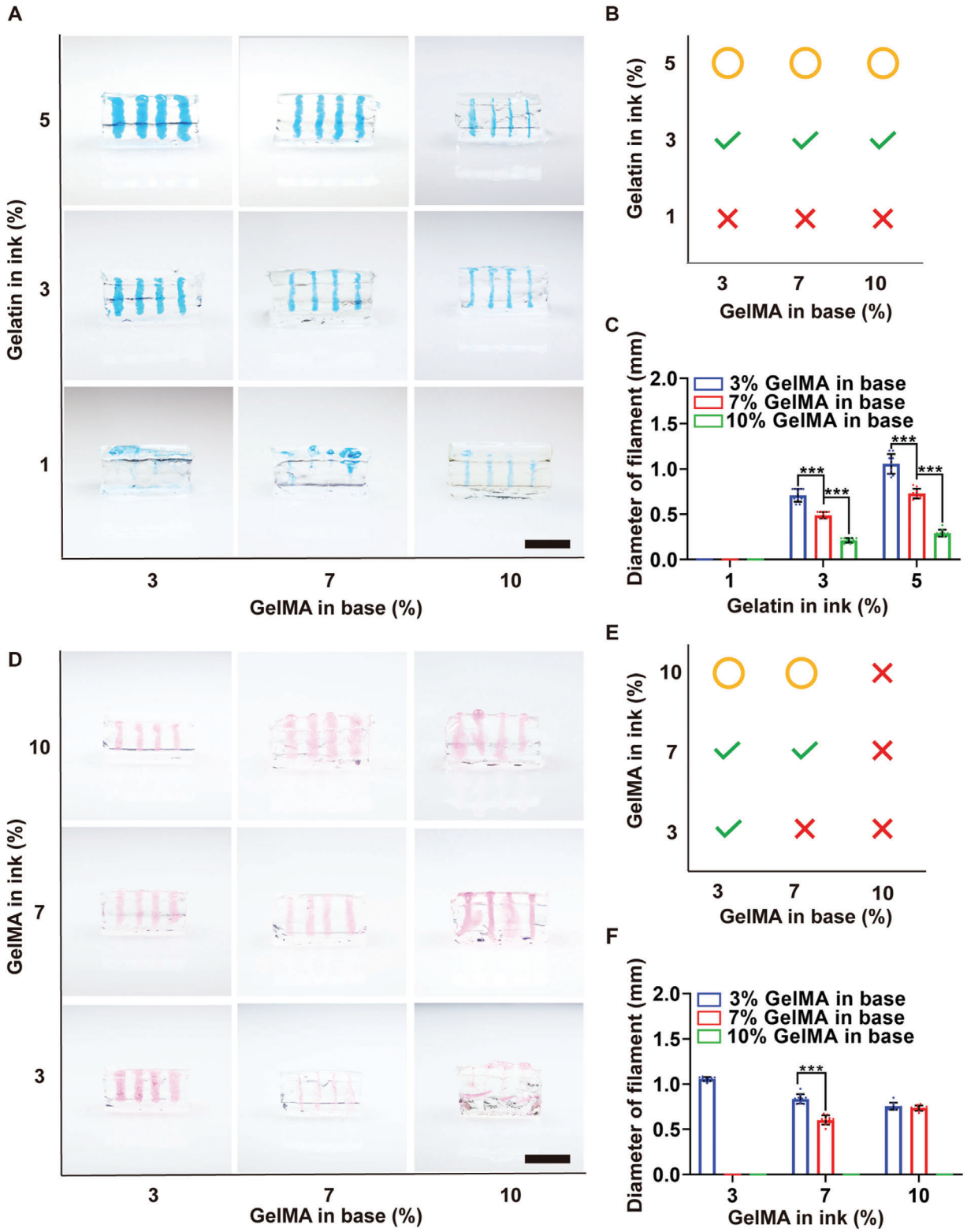

Figure 1. Printability evaluations of gelatin and GelMA (bio)inks for uniaxial vertical embedded (bio)printing. A) Filaments printed with different concentrations of gelatin as the (bio)ink using the uniaxial nozzle in different concentrations of GelMA support bases. Scale bar: 5 mm. B) Printability map of the gelatin (bio)ink; √: printable with uniform filament, O: printable with nonuniform filament, X: nonprintable. C) Corresponding quantified diameters of filaments. D) Filaments printed with different concentrations of GelMA as the (bio)ink using the uniaxial nozzle in different concentrations of GelMA support bases. Scale bar: 5 mm. E) Printability map of the GelMA (bio)ink; √: printable with uniform filament, O: printable with nonuniform filament, X: nonprintable. F) Corresponding quantified diameters of filaments. $^{***}p < 0.001$, $^{**}p < 0.01$, and $^{*}p < 0.05$; $n = 10$.

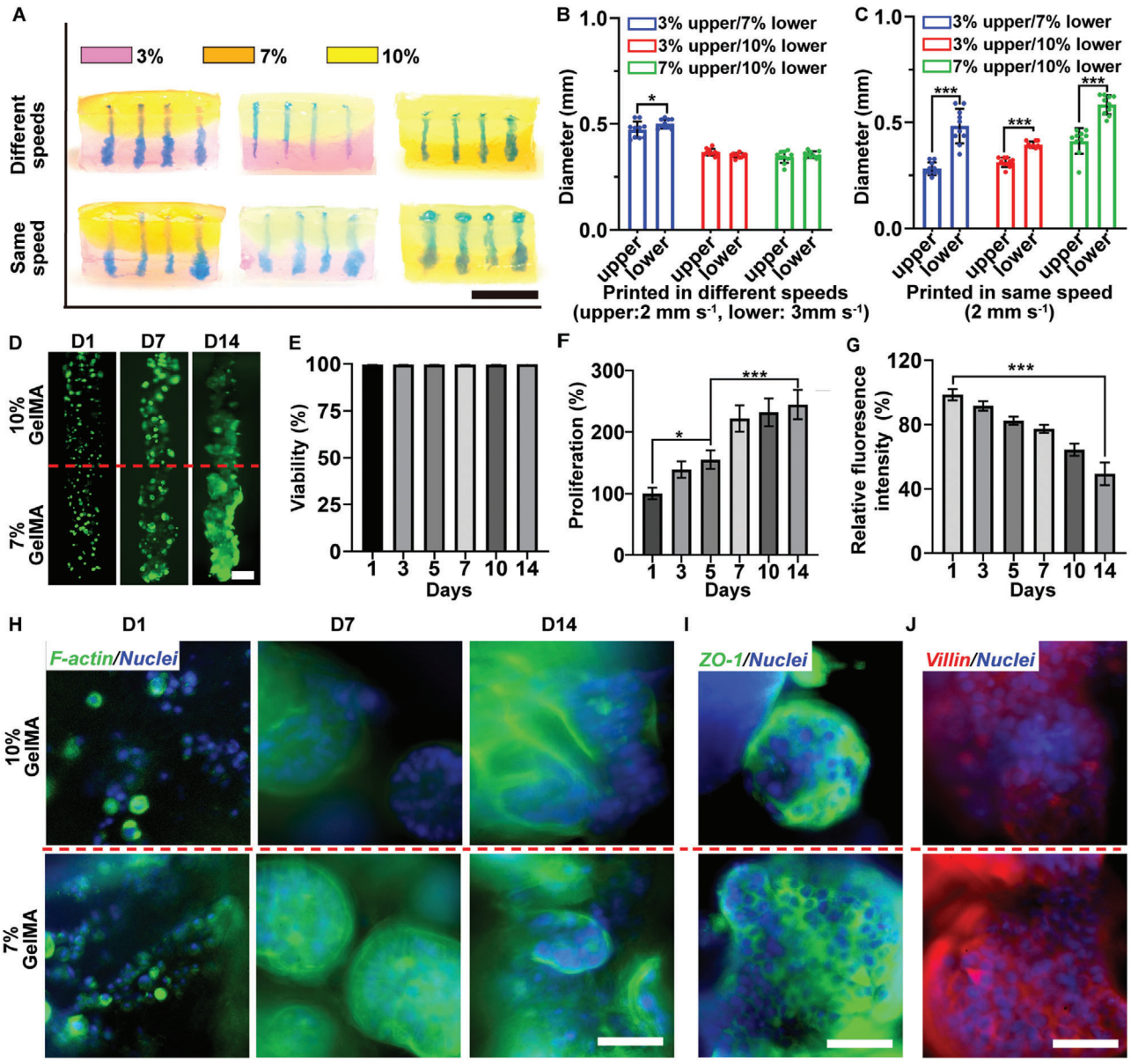

Figure 2. Uniaxial vertical embedded bioprinting of intestinal villi. A) Photographs showing the printing performances in dual-layered support baths: printing at different nozzle moving speeds (lower: 3 mm $^{-1}$, upper: 2 mm s^{-1}) or same speed (2 mm s^{-1}) of the uniaxial nozzle in different combinations of support bases. Scale bar: 5 mm. B) Quantified diameters of filament segments in the different layers when the nozzle was moved at different speeds (lower: 3 mm $^{-1}$, upper: 2 mm s^{-1}) ($n = 10$). C) Quantified diameters of filament segments in the different layers when the nozzle was moved at the same speed (2 mm s^{-1}) ($n = 10$). D) Live (green) and dead (red) images of Caco-2 cells vertical embedded-bioprinted in the dual-layered support base. Scale bar: 200 µm. E) Viability of Caco-2 cells at different days of culture ($n = 3$). F) Proliferation of Caco-2 cells at different days of culture ($n = 3$). G) Relative fluorescence intensities (ratio of the fluorescence intensities of the upper layer to those of the lower layer at the same time points) at different days of culture. H) Fluorescence micrographs of F-actin staining of the Caco-2 cells on days 1, 7, and 14 of culture. Scale bar: 100 µm. Fluorescence micrographs of I) ZO-1 and J) villin immunostaining of Caco-2 cells on day 14. Scale bars: 100 µm. Statistical significance is expressed as $^{***}p < 0.001$, $^{**}p < 0.01$, and $^{*}p < 0.05$.

the density of the polymer network, and thus its pore size, which is highly dependent on the concentration of the hydrogel.[43] According our previous results, the diffusivity of the 5% GelMA is 11 times higher than that of the 10% GelMA, if they have a same degree of methacryloyl-substitution and crosslinking time.[35] Therefore, we inferred that the microenvironment in the 10% GelMA of the upper layer and 7% GelMA of the lower layer possibly featured a massive difference (they both had the same degree of methacryloyl-substitution at ≈50% and crosslinking time at 30 s). This difference likely created a microenvironment gradient in terms of both nutrients and oxygen along the length of the intestinal villus structure that we bioprinted, in some ways mimicking the natural microenvironment of the native counterpart. Compared with other complicated culture devices equipped with

these microenvironment gradients[22,44,45] and conventional extrusion methods without the support base[46] for engineering the in vitro intestinal villus model, our vertical embedding bioprinting method with a concentration-gradient support bath could potentially pave a new way to produce heterogeneous microenvironmental cues at relative ease with improved precision.

Finally, cell confluency and barrier integrity are the two crucial parameters to form a functional epithelial model of the intestinal villi.[47] To validate the formation of a confluent Caco-2 cell layer, we assessed the cell–cell interactions by staining the samples with ZO-1, a junction maker after 14 days of culture. The result of the ZO-1 immunostaining demonstrated that both top and bottom layers had developed confluent epithelia with tight junctions (Figure 2I), where the overall areas of Caco-2 cells and their folds in the lower layer were larger than those in the upper layer. The observation indicated that this microenvironment gradient in the support base might have promoted Caco-2 cell expansion. Folding intestinal structures were also visible in some regions. In addition, the expression of villin, an epithelial brush border marker, was examined after culturing for 14 days. It was apparent that villin staining in the lower layer was more homogeneous than it was in the upper layer (Figure 2J), again revealing that the differential hydrogel densities in the surrounding microenvironment influenced the functional behaviors of Caco-2 cells along the same bioprinted vertical villus spaces. The semiquantitative results of ZO-1 and villin immunostaining fluorescence intensities are shown in Figure S3B (Supporting Information).

2.3. Optimization of Vertical Coaxial Embedded Bioprinting

Compared to vertical uniaxial embedded bioprinting, coaxial bioprinting is a more complicated process because two (bio)inks need to be extruded into the right locations of the support base during a single printing procedure with accurate dispensing of volumes and ratios. The printing parameters, including size and moving speed of the nozzles as well as pressures applied to the two layers of the nozzles, would all require optimizations. The schematic illustration of the customized coaxial nozzle is shown in **Figure 3**A.[48,49] To print a uniform vertical structure along the *z*-direction, the needles assembled should ideally be strictly concentric. Here, we listed three examples of different combinations of the nozzles in Figure 3B, where the printing performances of these coaxial nozzles are displayed in Figure S4A (Supporting Information). After comparing the diameters of the extruded filaments in Figure S4B (Supporting Information), the nozzle (30G internal and 22G external) in Figure 3B-i was chosen because the diameter printed was closest to that of the real hair follicles (268.41 ± 24.88 μm).[50,51]

We adopted 7% GelMA as the support base and formulation of one of the (bio)inks, because our preliminary evaluations of hFb behaviors in different concentrations of GelMA (3%, 7%, and 10%) showed better growth in 7% GelMA than in 3% and 10% GelMA (Figure S5A, Supporting Information). However, the viability of the cells did not reveal significant differences across the samples (Figure S5B, Supporting Information), consistent with the good cytocompatible property of GelMA widely reported.[52,53] In addition, the 3% gelatin was utilized as the other (bio)ink due to the need to support sacrificial performance for hKCs.

The potential impacts of (bio)ink composition on printing outcomes were further assessed. The two (bio)inks (3% gelatin and 7% GelMA) were evaluated separately, where the gelatin (bio)ink was extruded from the external channel of the nozzle while the GelMA (bio)ink was delivered through the internal channel. As shown in Figure 3C, the sizes of the filaments printed with the 3% gelatin (bio)ink changed when different extrusion pressures and nozzle moving speeds were applied. The diameters of the filaments increased with the rise of the extrusion pressure (Figure 3D); the lengths of the filaments decreased with the increase of the nozzle moving speed (Figure 3E). For the 7% GelMA (bio)ink, the same trends were observed (Figure 3F–H). A typical vertical embedded printing process including both segments using the coaxial nozzle was recorded (Movie S1, Supporting Information). Of note, while it is also possible to use two separate nozzles to achieve the sequential extrusion of heterogeneous filaments as demonstrated here, the single-nozzle yet coaxial design we used could be much more convenient and robust due to minimum disturbances when switching the (bio)ink.[54]

2.4. Hair Follicle Bioprinting

hDPCs are a type of mesenchymal cells that are highly specialized and play an indispensable role in the morphogenesis and functions of hair follicles.[55] To maintain the hair-inductivity of hDPCs, they shall be cocultured with keratinocytes in the right configuration and allowed to self-aggregate.[56] In addition, the size of dermal papilla changes varies with hair follicles at different sites, such as the facial skin and scalp.[57] Consequently, adjusting the proportion, shape, and size of hDPC-laden bottom portion in a filament would be important to attain relevant functions of the resulting hair follicle potentially in a location-dependent manner.

Interestingly, by controlling of the printing parameters (i.e., moving speed of the coaxial nozzle and extrusion pressures), the proportion and the diameter of the two segments of a single filament, could be readily adjusted using our coaxial nozzle setup, as schematized in **Figure 4**A,B. Shown in Figure 4C, the proportion of the bottom GelMA (bio)ink in the filament gradually changed with different moving speeds of the nozzle (from 1 to 4 mm s^{-1} at an interval of 1 mm s^{-1}) while the nozzle moving speed of the gelatin (bio)ink printing was kept at 1 mm s^{-1}. The quantified proportion of the bottom GelMA (bio)ink in the filament shown in Figure 4D indicated that it decreased with the increase of the nozzle moving speed. We further printed filaments featuring the bottom GelMA (bio)ink in different diameters (Figure 4E). When we kept the extrusion pressure for the gelatin (bio)ink at 8 psi and raised the extrusion pressure (from 13 to 16 psi at an interval of 1 psi) for the bottom GelMA (bio)ink, the diameter of the bottom GelMA (bio)ink increased gradually (Figure 4F). According to the size of typical actual hair follicles (diameter of ≈250 μm, length of ≈4 mm, and dermal papilla occupies ≈5–20% of the length),[14] structures printed with 1 mm s^{-1} of nozzle moving speed in both hDPC and hKC segments exhibited a high degree of similarity, coupled with 8 psi of pressure for gelatin (hKC) in the external channel and 14 psi for GelMA (hDPC) in the internal channel.

Cells were further laden into the bioinks to showcase the dual-material vertical embedded bioprinting process for producing the hair follicles. hDPCs (laden in the GelMA bioink) stained with

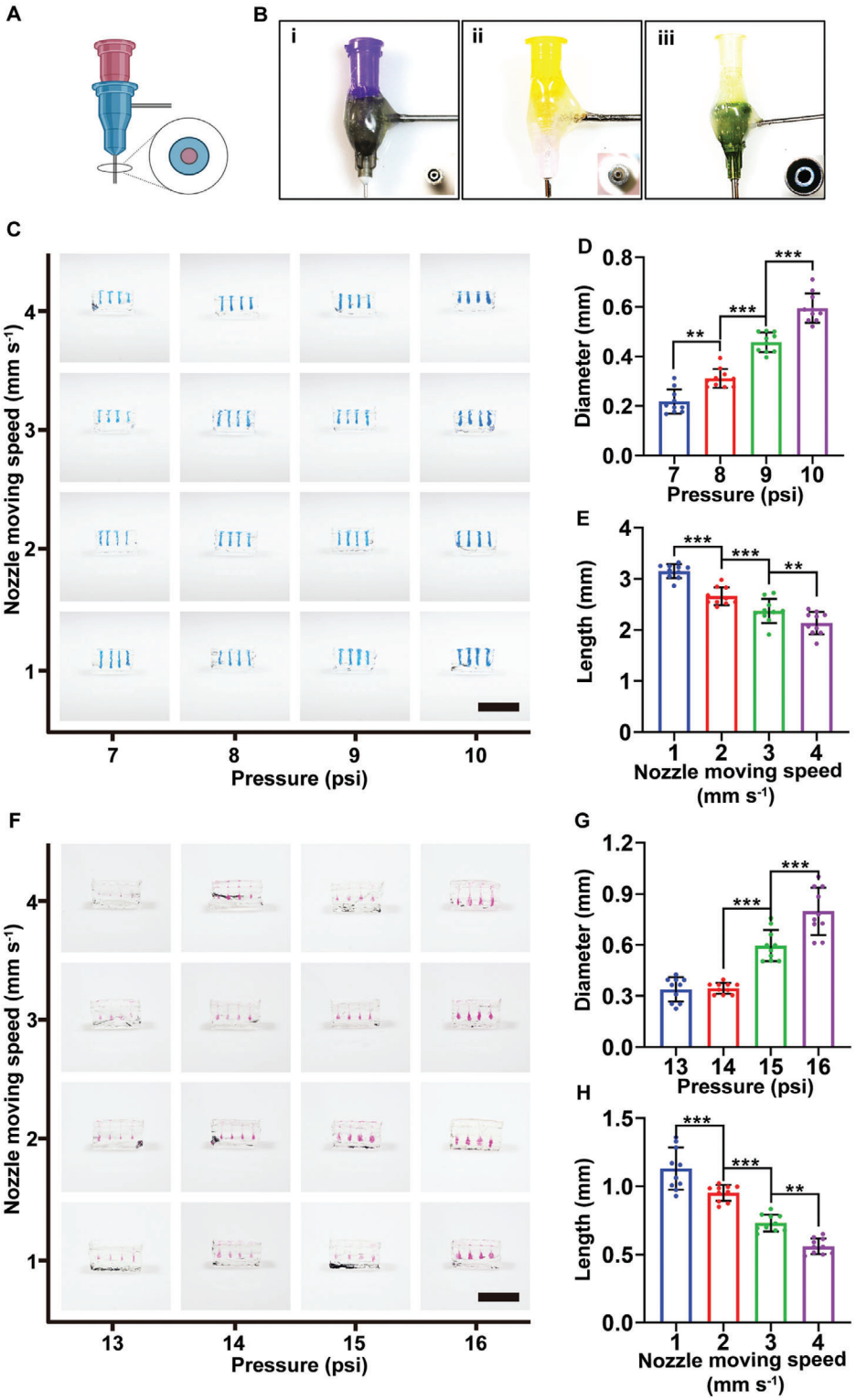

Figure 3. Optimization of coaxial vertical embedded (bio)printing. A) Scheme of the customized coaxial nozzle. B) Exemplary coaxial nozzles produced by needles of different size combinations: B-i) 30G for internal and 22G for external, B-ii) 25G for internal and 18G for external, and B-iii) 20G for internal and 14G for external. C) 3% gelatin (bio)ink printed in 7% GelMA support base at different extrusion pressures and nozzle moving speeds. Scale bar: 1 mm. D) Quantified diameters of filaments printed under different extrusion pressures. E) Quantified lengths of filaments printed under different nozzle moving speeds. F) 7% GelMA (bio)ink printed in 7% GelMA base at different extrusion pressures and nozzle moving speeds. Scale bar: 1 mm. G) Quantified diameters of filaments printed under different extrusion pressures. H) Quantified lengths of filaments printed under different nozzle moving speeds. Statistical significance is expressed as $^{***}p < 0.001$, $^{**}p < 0.01$, and $^{*}p < 0.05$; $n = 10$.

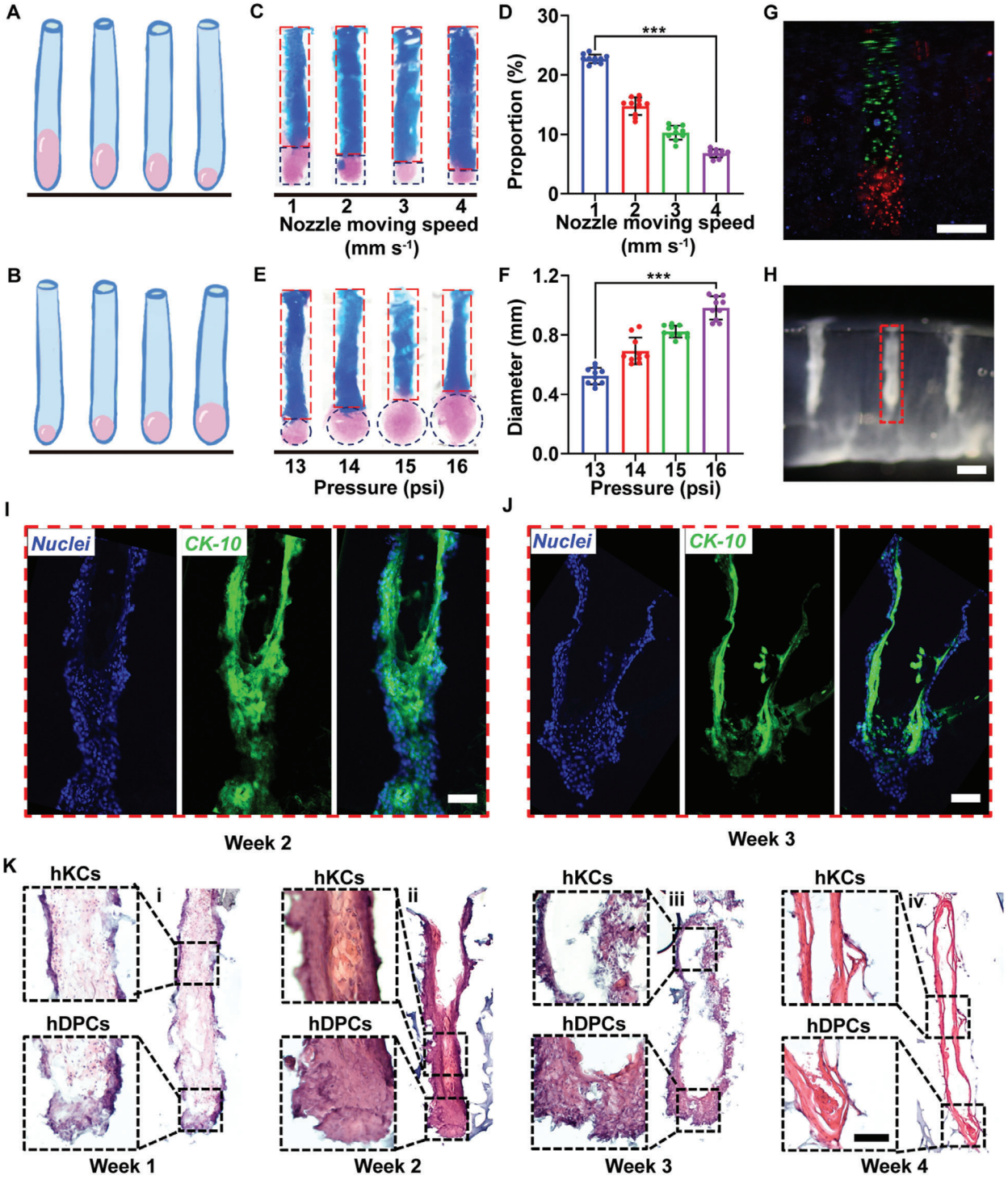

Figure 4. Coaxial vertical embedded bioprinting of hair follicles. A) Scheme showing different segment proportions of the filaments producible. B) Scheme showing different diameters of the lower segments producible. C) Printed filaments with different segment proportions as illustrated in (A) by changing the nozzle moving speed. D) Corresponding quantified proportions of the filament segments. E) Printed filaments with different lower segment diameters as illustrated in (B) by changing the extrusion pressure. F) Corresponding quantified diameters of the lower segments. G) Hair follicle bioprinting using 7% GelMA hDPC bioink (stained with red cell tracker) in the bottom segment and 3% gelatin hKC bioink (stained with green cell tracker) in the upper segment in a single filament within the hFb (stained with blue cell tracker)-laden 7% GelMA support base. Scale bar: 400 µm. H) Micrograph showing the gross appearance of the bioprinted hair follicle structure after culturing for 1 week. Scale bar: 400 µm. I) Immunostaining images showing CK-14 expression of the hair follicle-llike structure after culturing for 2 weeks. Scale bar: 200 µm. J) Immunostaining images showing CK-17 expression of the hair follicle-like structure after culturing for 3 weeks. Scale bar: 200 µm. K) H&E staining of the hair follicle structures after culturing for (i) 1, (ii) 2, (iii) 3, and (iv) 4 weeks. Scale bar: 200 µm. Statistical significance is expressed as $^{***}p < 0.001$, $^{**}p < 0.01$, and $^{*}p < 0.05$; $n = 10$.

red cell tracker and hKCs (laden in the gelatin bioink) stained with green cell tracker were co-bioprinted in the same, uniform 7% GelMA support base encapsulating hFbs, which were stained with the blue cell tracker (Figure 4G). This cell-laden support base and the coaxial bioprinting strategy precisely arranged the different types of cells into the target locations and established a microenvironment, which was anticipated to promote multiple cell–cell interactions as well as cellular lineage-specification. Compared with the previously reported, inverted molding method that seeded hKCs and hDPCs separately,[14] our vertical embedded bioprinting would likely improve the efficiency and accuracy of the spatial patterning process.

The bright-field micrograph of the hair follicle sample (Figure 4H) showed the status of filaments after culturing for 7 days with the co-culture growth medium. After culturing with EPI-I for 7 days, the tissue started to engulf the hDPC aggregate at the bottom and formed a hair follicle-like structure indicating with CK-14 positive hKCs (Figure 4I). The hDPCs were kept in the aggregate and hKCs expressed hair follicle marker CK-17 after further culturing with EPI-II for another 7 days (Figure 4J). Of note, the hKCs above the hDPC aggregate already started to show the similar differentiated morphology of these cells in the real hair follicles, reflecting the biomimetic configuration of the hKCs (epidermal) and hDPCs (mesenchymal). Prolonging the culture time more, the hKCs continued to keratinize and eventually formed a hollow structure, primarily aligning along the surface of the channel with the aid of the sacrificial gelatin bioink during the culture period (Figure 4J,K). At 4 weeks, the hKCs became almost entirely keratinized (Figure 4K-iv). The semi-quantified proportions of keratinized hKCs are shown in Figure S6 (Supporting Information).

Reconstruction of human hair follicles has been a long-standing challenge, especially with the increase of skin-related diseases where hair follicles are lost.[58] Developing an enabling platform equipped with desired cell types and spatial configurations for recreating the cell–cell interacting microenvironment and eventually hair growth, is the crucial progress to addressing this problem. The coaxial vertical embedded extrusion bioprinting method reported in this study provided a new strategy to establish such a platform in an efficient and precise manner. Although we were not able to obtain the fully differentiated hair follicle structure to support hair growth in vitro yet, the hair follicle-like structure with expressions of relevant biomarkers we bioprinted would serve as an initial key step toward engineering of physiologically relevant human hair follicles. Additional combination of transplantation[59] or gene editing[14] with our bioprinting method may allow the entire hair follicle structures to be developed, which we will pursue in the future.

3. Conclusion

In conclusion, we have developed a vertical embedded extrusion bioprinting technique using either uniaxial or coaxial nozzles, to produce high-aspect ratio vertical structures heterogeneous either within the filaments or within the surrounding matrices, to preliminarily mimic the intestinal villi and human hair follicles. Stable bioinks such as those based on GelMA and sacrificial bioinks such as gelatin could both be used to satisfy the requirements of the different tissues or tissue segments to be bioprinted. The method provided relatively complex microenvironments for these tissue types and allowed multiple bioinks or support bath layers to be used during single bioprinting processes, likely promoting cellular performances in the resulting structures. With further optimizations, such as co-extrusion in the co-axial nozzle to form core-shell vertical filaments with diameters of both layers adjustable (Figure S7, Supporting Information) rather than the sequential deposition demonstrated, it is believed that our strategy could be well-extended to the production of these reported tissues or other tissue types at high throughput for applications in regenerative medicine and tissue model engineering.

4. Experimental Section

Cells and Materials: HKCs and hFbs were isolated from human foreskin. HDPCs were isolated from discarded scalp tissues. The procedure for obtaining foreskin and adult scalp tissues from discarded hospital specimens without any personal identity information was approved by MassGeneralBrigham Human Research Committee (IRB protocol #2013P002158). Caco-2 cells were purchased from ATCC, USA. Hematoxylin, eosin, methacrylic anhydride, Triton X-100, bovine serum albumin (BSA), gelatin from porcine skin, 2-hydroxy-4′-(2-hydroxyethoxy)-2-methylpropiophenone (photoinitiator), dimethyl sulfoxide (DMSO), Y-27632 dihydrochloride, adenine, hydrocortisone, transferrin, insulin, progesterone, calcium chloride, formalin, and ethanol were purchased from Sigma-Aldrich, USA. Dulbecco's phosphate-buffered saline (DPBS), Dulbecco's modified Eagle medium (DMEM), keratinocyte serum-free medium (K-SFM), Ham's F-12K (Kaighn's) medium (F12), human epidermal growth factor (EGF) recombinant protein, B27 supplement, amphotericin B, L-glutamine, fetal bovine serum (FBS), penicillin–streptomycin (P/S), trypsin-ethylenediaminetetraacetic acid (EDTA), 4′,6-diamidino-2-phenylindole (DAPI), Live/Dead viability/cytotoxicity kit, PrestoBlue, Cell Trackers green CMFDA, CM-Dil, Blue-White DPX, Alexa Fluor 488-phalloidin, goat antirabbit IgG H&L (Alexa Fluor 488), goat antirabbit IgG H&L (Alexa Fluor 555), donkey antirabbit IgG H&L (Alexa Fluor 488), and dialysis membranes (M_w cutoff = 12000–14 000 Da) were purchased from Thermo Fisher Scientific, USA. Sterile syringe filters (0.22 µm in pore size) and vacuum filtration systems (0.22 µm in pore size) were purchased from VWR International, USA. Fluorescent color dyes were purchased from Create Colors, USA. Rabbit antihuman ZO1 antibody, rabbit antihuman villin antibody, rabbit anticytokeratin 14 (CK-14) antibody, and rabbit anticytokeratin 17 (CK-17) antibody were purchased from Abcam, USA. Needles of different sizes (14G, 18G, 20G, 22G, 25G, and 30G) were purchased from BD Biosciences, USA. Polydimethylsiloxane (PDMS, Sylgard 184) was purchased from Dow Inc., USA. DPX mounting medium was purchased from Agar Scientificm, USA. Optimal cutting temperature (OCT) compound was purchased from Sakura Finetek, USA. Superfrost microscope slides were purchased from Fisher Scientific, USA.

Synthesis of GelMA: GelMA was synthesized according to the established protocol[60,61] at a medium methacryloyl-substitution degree.[52,62] Briefly, type A gelatin from porcine skin was dissolved in DPBS at 10% (w/v unless otherwise noted) at 50 °C. Then methacrylic anhydride was added dropwise at a 0.5:1 weight ratio of anhydride to gelatin and the mixture was stirred at 50 °C for 2 h. The solution then was diluted with an equal volume of DPBS preheated to 50 °C and dialyzed with distilled water at 40 °C for 5 days. Finally, the solution was filtered by a vacuum filtration system and lyophilized.

Printability Assays and Optimizations of (Bio)printing Parameters: The bioprinter used was the Allevi 2 desktop 3D bioprinter (3D Systems, USA). G-codes for printing were edited in the Repetier-Host software (Hot-World GmbH & Co. KG, Germany). The support base-container was customized using PDMS.

GelMA at different concentrations (3%, 7%, and 10%) mixed with 0.3% photoinitiator served as the support bases. These support bases were cast into the PDMS containers. GelMA at different concentrations (3%, 7%,

and 10%) mixed with 0.3% photoinitiator and fluorescent color dye (pink) at a ratio of 1:2500 served as one of the (bio)inks. Gelatin at different concentrations (1%, 3%, and 5%) mixed with fluorescent color dye (blue) at a ratio of 1:2500 served as another (bio)ink type. Following the vertical embedded (bio)printing processes, the samples were photocrosslinked under UV light for 40 s. The photographs of the patterns were taken by a digital camera (70D, Canon, Japan) and analyzed to obtain the printability maps. The quantified diameter of each printed vertical filament was determined using ImageJ (National Institutes of Health, USA) ($n = 10$).

For further optimizing the parameters for the uniaxial vertical embedded printing process in a heterogeneous support base, the combinations of GelMA at different concentrations in different layers of the support base and the moving speed of the nozzle in the different layers were explored. There were three combinations of GelMA in the support bases (i.e., 7% GelMA in the lower layer and 10% GelMA in the upper layer, 3% GelMA in the lower layer and 10% GelMA in the upper layer, and 3% GelMA in the lower layer and 7% GelMA in the upper layer), again all cast into the PDMS containers. The 10% GelMA support base was mixed with fluorescent color dye (yellow), the 7% GelMA support base was mixed with fluorescent color dye (orange), and the 3% GelMA support base was mixed with fluorescent color dye (pink). The ink used for this uniaxial printing process was 3% gelatin (mixed with fluorescent color dye (blue)). The same moving speed (2 mm s^{-1}) to conduct printing in the different layers or different moving speeds (3 mm s^{-1} in the lower layer and 2 mm s^{-1} in the upper layer) was adopted. The diameters of the vertically embedprinted filaments in the different layers of the support base were measured using ImageJ from photographs taken ($n = 10$).

The printing parameters considered in the coaxial vertical embedded printing process were the moving speed of the coaxial nozzle and pressures applied to the two layers of the nozzle, similar to the processes that was used before in a similar setup concerning multimaterial embedded bioprinting.[63] Due to the dual-material printing process, the two inks were tested separately using the same customized coaxial nozzle. The ink used in the external channel was 3% gelatin (mixed with fluorescent color dye (blue)) and the ink delivered in the internal channel was 7% GelMA (mixed with 0.3% photoinitiator and fluorescent color dye (pink)). The gradual changes of the nozzle moving speed (1–4 mm s^{-1} at an interval of 1 mm s^{-1}) and pressure (7–9 psi for the external channel at an interval of 1 psi and 13–16 psi for the internal channel at an interval of 1 psi) provided different combinations for the printing processes. The diameters of the vertically printed filaments in the different layers of support base were measured using ImageJ from photographs taken ($n = 10$).

Preparation of Cells for Bioprinting: For intestinal villus bioprinting, the Caco-2 cells were cultured in DMEM containing 10% FBS and 0.1% P/S, and the growth medium was changed every 2 days. The Caco-2 cells were trypsinized by trypsin-EDTA when they reached ≈80% cell confluency and used for the following bioprinting process.

For hair follicle bioprinting, hKCs were cultured in K-SFM plus 5 $\times 10^{-6}$ M of Y-27632 dihydrochloride, and the medium was changed every 2 days. hDPCs were cultured in DMEM /F12 (3:1) containing 5% FBS, 0.1% P/S, 20 ng mL^{-1} of EGF, 40 µg mL^{-1} of amphotericin B, and 2% B27 supplement, and the growth medium was changed every 5 days. hKCs and hDPCs were trypsinized by trypsin-EDTA when they reached ≈80% cell confluency and used for the following bioprinting process.

Vertical Embedded Bioprinting of Intestinal Villi and Hair Follicles: For intestinal villus bioprinting, GelMA at different concentrations (7% for the lower layer and 10% for the upper layer) used for the support base was mixed with 0.3% photoinitiator and then filtered by sterile syringe filters. The bioink was prepared by filtering 3% gelatin using a sterile syringe filter and then mixing with Caco-2 cells (1×10^7 cells mL^{-1}) to load into the uniaxial nozzle.

For hair follicle bioprinting, 7% GelMA was mixed with 0.3% photoinitiator and filtered by a sterile syringe filter. The filtered 7% GelMA was separately mixed with hDPCs (1×10^7 cells mL^{-1}) as the bioink used in the internal channel of the coaxial nozzle and mixed with hFbs (5×10^6 cells mL^{-1}) as the support base. 3% gelatin filtered by a sterile syringe filter was mixed with hKCs (1×10^7 cells mL^{-1}) as the other bioink used in the external channel of the nozzle.

The intestinal villus structure in this study was bioprinted using a commercial uniaxial needle (30G), whereas the hair follicle structure was bioprinted using a customized coaxial nozzle that combined two different sizes of needles (30G internal and 22G external).

Cell Proliferation Assay: The metabolic activities of Caco-2 cell-laden vertical embedded-bioprinted intestinal villus samples were measured by the PrestoBlue on days 1, 3, 5, 7, 10, and 14 according to the manufacturer's instructions. After washing the samples twice with PBS, the samples were placed in the wells of a 48-well plate, where a working solution composed of the culture medium and the reagent at a proportion of 9:1 (v/v) was added into each well. After incubating for 3 h at 37 °C in the incubator, the supernatants were read by a spectrophotometer (excitation: 570 nm, emission: 600 nm; I-control, Tecan, Switzerland) to quantify ($n = 3$).

Cell Viability Assay: For intestinal villus bioprinting, viability of Caco-2 cells vertical embedded-bioprinted was measured by the Live/Dead viability/cytotoxicity kit on days 1, 3, 5, 7, 10, and 14 according to the manufacturer's instructions. For assessing the viability of hFbs in GelMA at different concentrations (3%, 5%, and 7%), the cells were stained using the same kit on days 1, 4, and 7 of culture. The fluorescence images were taken using a fluorescence microscope (Nikon E-Ti, Japan). The numbers of live and dead cells were counted using Image J. Cell viability was calculated by dividing the number of live cells by the total number of cells.

F-Actin and Immunostaining: For F-actin staining, intestinal villus samples were fixed on days 1, 7, and 14 with 10% formalin solution for 15 min at room temperature. The samples were then permeabilized with 0.1% Triton X-100 in PBS for 10 min at room temperature. After blocking with 1% BSA PBS solution at 4 °C overnight, the samples were incubated with Alexa Fluor 488-phalloidin PBS solution diluted at 1:1000 (v/v) at 4 °C overnight. After washing with PBS for three times, the samples were incubated with a DAPI PBS solution diluted at 1:2500 (v/v) for 15 min. The images were captured using the Nikon E-Ti fluorescence microscope.

For immunostaining of intestinal villus samples, they were fixed on day 14 with 10% formalin solution for 15 min at room temperature. The samples were then permeabilized with 0.1% Triton X-100 in PBS for 10 min at room temperature and blocked using 1% BSA PBS solution at 4 °C overnight. After washing with PBS for three times, the samples were incubated separately with two primary antibodies solutions (i.e., rabbit anti-ZO-1 antibody PBS solution diluted at 1:500 (v/v) and rabbit antivillin antibody PBS solution diluted at 1:500 (v/v)) at 4 °C overnight. The samples incubated with the rabbit anti-ZO-1 primary antibody were then treated with the secondary antibody solution (Alexa Fluor 488 goat antirabbit IgG H&L PBS solution diluted at 1:400 (v/v)) at room temperature for 2 h. The samples incubated with the rabbit antivillin primary antibody were treated with the secondary antibody solution (Alexa Fluor 555 goat antirabbit IgG H&L PBS solution diluted at 1:400 (v/v)) at room temperature for 2 h. The specimens were further incubated with the DAPI PBS solution diluted at 1:2500 (v/v) at room temperature for 15 min. The images were taken with the Nikon E-Ti fluorescence microscope and analyzed utilizing ImageJ.

After culturing with coculture growth medium which mixed the two types of medium for culturing hKCs and hDPCs at a ratio of 1:1 (v/v) for 7 days, the hair follicle samples were cultured with epidermalization I (EPI-I) for 7 days and then cultured with epidermalization II (EPI-II) for 2 weeks. EPI-I was prepared by adding 4 $\times 10^{-3}$ M of L-glutamine, 40 $\times 10^{-6}$ M of adenine, 1% hydrocortisone, 10 µg mL^{-1} of transferrin, 10 µg mL^{-1} of insulin, and 2 $\times 10^{-9}$ M of progesterone to DMEM /F12 (3:1) and EPI-II by adding 1.8 $\times 10^{-3}$ M of calcium chloride to EPI-I, following the previous study.[64] The immunostaining of hair follicle samples was taken at weeks 2 and 3. Specifically, for immunostaining of the hair follicle constructs, after fixing with 10% formalin for 15 min at room temperature, the samples were embedded in OCT compound and frozen at −20 °C. The samples were subsequently sliced (30 µm) onto superfrost microscope slides using a cryostat (CM 1850, Leica, Germany). The cryosections were incubated with the blocking buffer (mixed 2% BSA, 0.01% Triton X-100, and 5% donkey serum in PBS) at room temperature for 1 h. The blocked samples obtained at week 2 were incubated with the primary antibody solution (rabbit anti-CK14 antibody PBS solution diluted at 1:400 (v/v)) at 4 °C overnight, and the samples treated at week 3 were then incubated with the primary

antibody solution (rabbit anti-CK17 antibody PBS solution diluted at 1:400 (v/v)) at 4 °C overnight. Afterward, the specimens were incubated with the secondary antibody solution (Alexa Fluor 488donkey antirabbit IgG H&L PBS solution diluted at 1:400 (v/v)) at room temperature for 1 h. After washing using PBS for three times, the samples were mounted using the DPX mounting medium. The images were captured and analyzed using a confocal microscope (TCS SP5, Leica, Germany).

Hematoxylin and Eosin (H&E) Staining: The cryo-sectioned hair follicle samples were stained with hematoxylin at room temperature for 3 min. Blue staining was developed by rinsing under tap water for 1 min, and counterstaining was performed by immersing the slices with eosin for 30 s and ringing again under tap water for 1 min. The dehydrated samples were obtained by sequential immersion in 50%, 70%, 90%, and 100% ethanol for 1 min each. The dehydrated samples were treated with toluene and xylene for 1 min each and covered with coverslips with the aid of the DPX mounting medium, and examined with light microscopy using the Zeiss Axioplan 2 microscope.

Statistical Analyses: All data were indicated as means ± standard deviations (SDs) for $n \geq 3$. GraphPad Prism (GraphPad Software, USA) was used to perform a two-way analysis of variance (ANOVA) with Tukey's post hoc multiple comparison test to determine statistical significance ($^{*}p \leq 0.05$, $^{**}p \leq 0.01$, $^{***}p \leq 0.001$).

Supporting Information

Supporting Information is available from the Wiley Online Library or from the author.

Acknowledgements

L.L., C.Z., and G. T. contributed equally to this work. The authors acknowledge the support by the Brigham Research Institute.

Conflict of Interest

Y.S.Z. sits on the Advisory Board of Allevi, Inc., which however, did not support this work. The other authors declare no competing interests.

Data Availability Statement

The data that support the findings of this study are available from the corresponding author upon reasonable request.

Keywords

bioprinting, coaxial, embedded, multimaterial, tissue engineering, vertically

Received: November 6, 2021
Revised: November 22, 2021
Published online:

[1] A. B. Dababneh, I. T. Ozbolat, *J. Manuf. Sci. Eng.* **2014**, *136*, 061016.
[2] J. Groll, T. Boland, T. Blunk, J. A. Burdick, D.-W. Cho, P. D. Dalton, B. Derby, G. Forgacs, Q. Li, V. A. Mironov, L. Moroni, M. Nakamura, W. Shu, S. Takeuchi, G. Vozzi, T. B. F. Woodfield, T. Xu, J. J. Yoo, J. Malda, *Biofabrication* **2016**, *8*, 013001.
[3] S. V. Murphy, A. Atala, *Nat. Biotechnol.* **2014**, *32*, 773.
[4] M. A. Heinrich, W. Liu, A. Jimenez, J. Yang, A. Akpek, X. Liu, Q. Pi, X. Mu, N. Hu, R. M. Schiffelers, J. Prakash, J. Xie, Y. S. Zhang, *Small* **2019**, *15*, 1805510.
[5] R. Levato, T. Jungst, R. G. Scheuring, T. Blunk, J. Groll, J. Malda, *Adv. Mater.* **2020**, *32*, 1906423.
[6] X. Li, B. Liu, B. Pei, J. Chen, D. Zhou, J. Peng, X. Zhang, W. Jia, T. Xu, *Chem. Rev.* **2020**, *120*, 10793.
[7] W. Liu, Z. Zhong, N. Hu, Y. Zhou, L. Maggio, A. K. Miri, A. Fragasso, X. Jin, A. Khademhosseini, Y. S. Zhang, *Biofabrication* **2018**, *10*, 024102.
[8] P. S. Gungor-Ozkerim, I. Inci, Y. S. Zhang, A. Khademhosseini, M. R. Dokmeci, *Biomater. Sci.* **2018**, *6*, 915.
[9] Y. S. Zhang, G. Haghiashtiani, T. Hübscher, D. J. Kelly, J. M. Lee, M. Lutolf, M. C. Mcalpine, W. Y. Yeong, M. Zenobi-Wong, J. Malda, *Nat. Rev. Methods Primers* **2021**, *1*, 75.
[10] W. Li, M. Wang, L. S. Mille, J. A. Robledo Lara, V. Huerta, T. Uribe Velazquez, F. Cheng, H. Li, J. Gong, T. Ching, C. A. Murphy, A. Lesha, S. Hassan, T. B. F. Woodfield, K. S. Lim, Y. S. Zhang, *Adv. Mater.* **2021**, *33*, 2102153.
[11] M. Wang, W. Li, L. S. Mille, T. Ching, Z. Luo, G. Tang, C. E. Garciamendez, A. Lesha, M. Hashimoto, Y. S. Zhang, *Adv. Mater.* **2021**, 2107038.
[12] Z. Liang, Y. Pei, C. Chen, B. Jiang, Y. Yao, H. Xie, M. Jiao, G. Chen, T. Li, B. Yang, L. Hu, *ACS Nano* **2019**, *13*, 12653.
[13] W. Kim, G. H. Kim, *Chem. Eng. J.* **2018**, *334*, 2308.
[14] H. E. Abaci, A. Coffman, Y. Doucet, J. Chen, J. Jackow, E. Wang, Z. Guo, J. U. Shin, C. A. Jahoda, A. M. Christiano, *Nat. Commun.* **2018**, *9*, 5301.
[15] J. Lee, C. C. Rabbani, H. Gao, M. R. Steinhart, B. M. Woodruff, Z. E. Pflum, A. Kim, S. Heller, Y. Liu, T. Z. Shipchandler, K. R. Koehler, *Nature* **2020**, *582*, 399.
[16] T. Sato, R. G. Vries, H. J. Snippert, M. Van De Wetering, N. Barker, D. E. Stange, J. H. Van Es, A. Abo, P. Kujala, P. J. Peters, H. Clevers, *Nature* **2009**, *459*, 262.
[17] O. Kwon, T. S. Han, M. Y. Son, *Front Cell Dev. Biol.* **2020**, *8*, 593969.
[18] C. K. Sen, G. M. Gordillo, S. Roy, R. Kirsner, L. Lambert, T. K. Hunt, F. Gottrup, G. C. Gurtner, M. T. Longaker, *Wound Repair Regen.* **2009**, *17*, 763.
[19] J. Creff, L. Malaquin, A. Besson, *J. Tissue Eng.* **2021**, *12*, 2041731420985202.
[20] S. S. Hinman, R. Kim, Y. Wang, K. S. Phillips, P. J. Attayek, N. L. Allbritton, *Curr. Opin. Biomed. Eng.* **2020**, *13*, 94.
[21] C. M. Costello, J. Hongpeng, S. Shaffiey, J. Yu, N. K. Jain, D. Hackam, J. C. March, *Biotechnol. Bioeng.* **2014**, *111*, 1222.
[22] R. Kim, P. J. Attayek, Y. Wang, K. L. Furtado, R. Tamayo, C. E. Sims, N. L. Allbritton, *Biofabrication* **2019**, *12*, 015006.
[23] H. Clevers, *Cell* **2013**, *154*, 274.
[24] J. Visser, B. Peters, T. J. Burger, J. Boomstra, W. J. A. Dhert, F. P. W. Melchels, J. Malda, *Biofabrication* **2013**, *5*, 035007.
[25] H. Ravanbakhsh, V. Karamzadeh, G. Bao, L. Mongeau, D. Juncker, Y. S. Zhang, *Adv. Mater.* **2021**, *33*, 2104730.
[26] L. Ning, R. Mehta, C. Cao, A. Theus, M. Tomov, N. Zhu, E. R. Weeks, H. Bauser-Heaton, V. Serpooshan, *ACS Appl. Mater. Interfaces* **2020**, *12*, 44563.
[27] M. Rocca, A. Fragasso, W. Liu, M. A. Heinrich, Y. S. Zhang, *SLAS Technol.* **2018**, *23*, 154.
[28] A. M. Compaan, K. Song, W. Chai, Y. Huang, *ACS Appl. Mater. Interfaces* **2020**, *12*, 7855.
[29] K. Troendle, L. Rizzo, R. Pichler, F. Koch, A. Itani, R. Zengerle, S. S. Lienkamp, P. Koltay, S. Zimmermann, *Biofabrication* **2021,** 13, 035019.
[30] W. Liu, M. A. Heinrich, Y. Zhou, A. Akpek, N. Hu, X. Liu, X. Guan, Z. Zhong, X. Jin, A. Khademhosseini, Y. S. Zhang, *Adv. Healthcare Mater.* **2017**, 6, 1601451.

[31] G. Ying, N. Jiang, C. Yu, Y. S. Zhang, *Bio-Des. Manuf.* **2018**, *1*, 215.
[32] E. Allen-Vercoe, *Curr. Opin. Microbiol.* **2013**, *16*, 625.
[33] J. B. Ward, S. J. Keely, S. J. Keely, *J. Physiol.* **2014**, *592*, 2473.
[34] D. Kachlik, V. Baca, J. Stingl, *J. Anat.* **2010**, *216*, 335.
[35] A. K. Miri, H. G. Hosseinabadi, B. Cecen, S. Hassan, Y. S. Zhang, *Acta Biomater.* **2018**, *77*, 38.
[36] A. G. Castano, M. Garcia-Diaz, N. Torras, G. Altay, J. Comelles, E. Martinez, *Biofabrication* **2019**, *11*, 025007.
[37] C. A. Higgins, J. C. Chen, J. E. Cerise, C. A. Jahoda, A. M. Christiano, *Proc. Natl. Acad. Sci. USA* **2013**, *110*, 19679.
[38] A. T. Young, O. C. White, M. A. Daniele, *Macromol. Biosci.* **2020**, *20*, 2000183.
[39] S. M. Bittner, H. A. Pearce, K. J. Hogan, M. M. Smoak, J. L. Guo, A. J. Melchiorri, D. W. Scott, A. G. Mikos, *Tissue Eng., Part A* **2021**, *27*, 665.
[40] S. Ozturk Mehmet, K. Lee Vivian, H. Zou, H. Friedel Roland, X. Intes, G. Dai, *Sci. Adv. 6*, eaay7513.
[41] D. J. Brayden, *J. Pharm. Sci.* **2021**, *110*, 12.
[42] H. Kaur, A. Erickson, R. Moreau, *Life Sci.* **2021**, *284*, 119920.
[43] P. Eiselt, J. Yeh, R. K. Latvala, L. D. Shea, D. J. Mooney, *Biomaterials* **2000**, *21*, 1921.
[44] D. Ulluwishewa, R. C. Anderson, W. Young, W. C. Mcnabb, P. Van Baarlen, P. J. Moughan, J. M. Wells, N. C. Roy, *Cell. Microbiol.* **2015**, *17*, 226.
[45] E. Maier, R. C. Anderson, N. C. Roy, *Nutrients* **2017**, *9*, 1349.
[46] W. Kim, G. H. Kim, *Theranostics* **2020**, *10*, 2495.
[47] J. Huang, Y. Ren, X. Wu, Z. Li, J. Ren, *J. Tissue Eng.* **2019**, *10*, 2041731419839846.
[48] J. Gong, C. C. L. Schuurmans, A. M. V. Genderen, X. Cao, W. Li, F. Cheng, J. J. He, A. Lopez, V. Huerta, J. Manriquez, R. Li, H. Li, C. Delavaux, S. Sebastian, P. E. Capendale, H. Wang, J. Xie, M. Yu, R. Masereeuw, T. Vermonden, Y. S. Zhang, *Nat. Commun.* **2020**, *11*, 1267.
[49] Q. Pi, S. Maharjan, X. Yan, X. Liu, B. Singh, A. M. Van Genderen, F. Robledo-Padilla, R. Parra-Saldivar, N. Hu, W. Jia, C. Xu, J. Kang, S. Hassan, H. Cheng, X. Hou, A. Khademhosseini, Y. S. Zhang, *Adv. Mater.* **2018**, *30*, 1706913.
[50] N. Otberg, H. Richter, H. Schaefer, U. Blume-Peytavi, W. Sterry, J. Lademann, *J. Invest. Dermatol.* **2004**, *122*, 14.
[51] A. Ishino, T. Takahashi, J. Suzuki, Y. Nakazawa, T. Iwabuchi, M. Tajima, *Br. J. Dermatol.* **2014**, *171*, 1052.
[52] K. Yue, X. Li, K. Schrobback, A. Sheikhi, N. Annabi, J. Leijten, W. Zhang, Y. S. Zhang, D. W. Hutmacher, T. J. Klein, A. Khademhosseini, *Biomaterials* **2017**, *139*, 163.
[53] F. Zhou, Y. Hong, R. Liang, X. Zhang, Y. Liao, D. Jiang, J. Zhang, Z. Sheng, C. Xie, Z. Peng, X. Zhuang, V. Bunpetch, Y. Zou, W. Huang, Q. Zhang, E. V. Alakpa, S. Zhang, H. Ouyang, *Biomaterials* **2020**, *258*, 120287.
[54] W. Liu, Y. S. Zhang, M. A. Heinrich, F. De Ferrari, H. L. Jang, S. M. Bakht, M. M. Alvarez, J. Yang, Y.-C. Li, G. Trujillo-De Santiago, A. K. Miri, K. Zhu, P. Khoshakhlagh, G. Prakash, H. Cheng, X. Guan, Z. Zhong, J. Ju, G. H. Zhu, X. Jin, S. R. Shin, M. R. Dokmeci, A. Khademhosseini, *Adv. Mater.* **2017**, *29*, 1604630.
[55] K. E. Toyoshima, K. Asakawa, N. Ishibashi, H. Toki, M. Ogawa, T. Hasegawa, T. Irie, T. Tachikawa, A. Sato, A. Takeda, T. Tsuji, *Nat. Commun.* **2012**, *3*, 784.
[56] A. J. Reynolds, C. A. Jahoda, *Development* **1996**, *122*, 3085.
[57] K. Elliott, T. J. Stephenson, A. G. Messenger, *J. Invest. Dermatol.* **1999**, *113*, 873.
[58] A. R. Castro, E. Logarinho, *Stem Cells Transl. Med.* **2020**, *9*, 342.
[59] C. A. Jahoda, K. A. Horne, R. F. Oliver, *Nature* **1984**, *311*, 560.
[60] S. Maharjan, D. Bonilla, P. Sindurakar, H. Li, W. Li, S. Duarte, A. Zarrinpar, Y. S. Zhang, *Bio-Des. Manuf.* **2021**, *4*, 157.
[61] D. Huang, T. Liu, J. Liao, S. Maharjan, X. Xie, M. Perez, I. Anaya, S. Wang, A. Tirado Mayer, Z. Kang, W. Kong, V. L. Mainardi, C. E. Garciamendez-Mijares, G. Garcia Martinez, M. Moretti, W. Zhang, Z. Gu, A. M. Ghaemmaghami, Y. S. Zhang, *Proc. Natl. Acad. Sci. USA* **2021**, *118*, 2016146118.
[62] M. Zhu, Y. Wang, G. Ferracci, J. Zheng, N. J. Cho, B. H. Lee, *Sci. Rep.* **2019**, *9*, 6863.
[63] M. Rocca, A. Fragasso, W. Liu, M. A. Heinrich, Y. S. Zhang, *SLAS Technol.* **2017**, *23*, 154.
[64] M. W. Carlson, A. Alt-Holland, C. Egles, J. A. Garlick, *Curr. Protoc. Cell Biol.* **2008**, *41*, 19.9.